RESEARCH ON THE DEFORMATION BEHAVIOR AND RESTORING MODEL OF ENERGY-SAVING BLOCK & INVISIBLE MULTI-RIBBED FRAME WALLS

S.C. Li[1], J.X. Dong[2] and L.F. Li[2]

[1]*Professor, School of Civil Engineering, Huaqiao University, Quanzhou. China*

[2]*graduate student, School of Civil Engineering, Huaqiao University, Quanzhou. China*

Email: lsc50605@hqu.edu.cn, xueyang@hqu.edu.cn, lilifeng@hqu.edu.cn

ABSTRACT: Six pieces of energy-saving block and invisible multi-ribbed frame walls of 1/2 scale were tested through pseudo static test. Based on the test results, hysteretic curves of shear force and displacement of the models were obtained and discussed. A general skeleton curve of shear force and displacement was formed on the basis of the hysteretic curves. The restoring model for the analysis of earthquake response of the energy-saving block and invisible multi-ribbed frame walls was eventually proposed. The deformation behavior of the specimens was discussed, and formulas for calculating the rigidity of the walls at different loading stages were proposed as well. The research showed that average lateral displacement ductility factor of the energy-saving block and invisible multi-ribbed frame walls calculated by test results was 3.16. This value illustrates the walls appropriately designed can fully meet the seismic requirement of the structures. Deteriorative quadrilinear restoring model of the walls fitted by test results can quite accurately reflect hysteretic behaviors and skeleton curves of the walls, and it can be applied to energy-saving block and invisible multi-ribbed structural earthquake response analysis.

KEYWORDS: energy-saving block and invisible multi-ribbed frame wall, pseudo static test, deformation behavior, rigidity, restoring model

1. INTRODUCTION

The energy-saving block and invisible multi-ribbed frame wall is a new structural bearing member with perfect properties such as light weight, high strength, low energy consumption and good seismic capacity . This kind of wall is composed of insulation energy-saving block and invisible multi-ribbed frame, whose bearing force property and seismic performance differ from the common concrete member. In this paper, six 1/2 scale specimen models were tested under cyclic horizontal loads to study the deformation performance and restoring model.

2. TEST SPECIMENS AND PROCEDURE

In the test, three groups of 1/2 scale specimen models, two pieces per group, were designed; one of which is with C20 fine stone concrete and the other with M20 high strength mortar when pouring the rib columns and beams. The specimen model is composed of insulation energy-saving block and invisible multi-ribbed frame. The

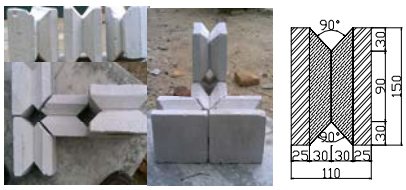

Figure1 Abridged general view of the blocks and the combination form

Foundation item: The research and development project of Ministry of Construction, P.R. China(06-k3-17); Scientific and technological planning project of Xiamen city(3502Z20073035); Key scientific and technological planning project of Fujian province(2008H0029); Natural science foundation planning project of Fujian province(E0810022)

block is aerated concrete block mainly using industry waste as materials such as coal ash, furnace slag and so on (the general view of blocks is shown in Figure 1).There is one v-groove in every side of the blocks except the front and rear, which was for pouring the invisible reinforced concrete column (the prism with a diagonal of 60mm long) and beam (the same size as the column) to eventually form the invisible multi-ribbed frame. A large outer frame around the small concrete frame (shown in Figure 2) was formed by increasing the diameter of reinforcing steel bars at the junction of the main wall and the wing wall as well as the junction of the top (bottom) beam and the main wall. The reinforcement arrangement is shown in Table 1.

The loading set-up is shown in Figure 3. Considering the worst-case stress state, the low-cycle reversed lateral loading system is adopted on the basis of the comprehensive analysis of the test objectives and the loading equipment. The horizontal load is applied on the top beam's loading end by hydraulic actuator connected to reaction frame. The procedure was a displacement control method. The number of cycles is only once for each incremental displacement step before the specimen yields. After yielding appears, the number of cycles for each incremental displacement is two till the specimen failure.

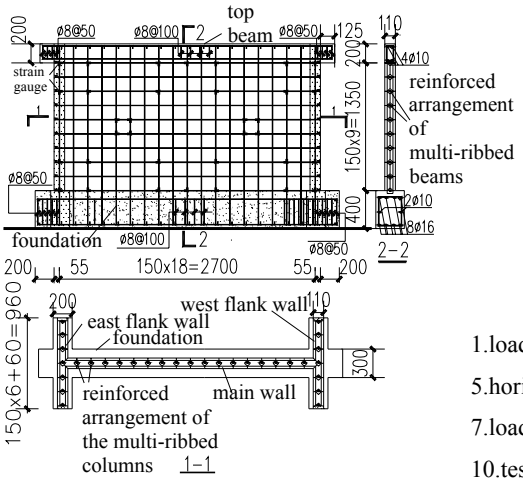

Figure 2 Multi-ribbed frame wall

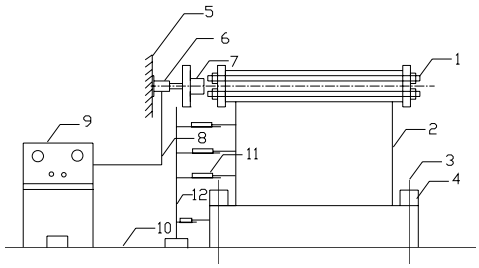

1.loading steel beam 2.specimen 3.anchor bolt 4.pressure beam
5.horizontal loading support frame 6.horizontal loading actuator
7.loading sensor 8.pipeline 9.Hydraulic Loading console
10.test platform 11.displacement meter 12.calibrating support

Figure 3 Loading set-up

Table 1 Design of specimens

Specimen number	Reinforced arrangement(HPB235)			
	Exterior rib column	Interior rib column	Top/bottom rib beam	Interior rib beam
EW1-1 EW1-2	1ϕ8	1ϕ6	1ϕ8	1ϕ6
EW2-1 EW2-2	1ϕ10	1ϕ8	1ϕ8	1ϕ6
EW3-1 EW3-2	2ϕ8	2ϕ6	1ϕ10	1ϕ8

3. HYSTERETIC CHARACTERISTICS AND AVERAGE SKELETON CURVES

3.1. Hysteretic Curves

(1) Hysteretic curves' intercommunity of model walls

From the hysteretic curves shown in Figure 4, it can be seen that the deformation of the model walls mainly represents elastic and the curves of shear force and displacement basically display the linear speciality before initial cracking of the aerated concrete block. The rigidity of model walls degenerate slightly as the wall initially cracked and the hysteretic loop's area is very small when unloading. As the load increasing, the cracks became more and more, and the hysteretic curves pinched to a certain extent but not very severe when unloading to zero. Meanwhile, the hysteretic curves present the lunar shape, which means that no obvious shear deformation and slippage occurred. When loading continuously to the ultimate load, the rigidity of model walls has degenerated obviously, the hysteretic loops plumped and pinched significantly near the origin of coordinates, and the hysteretic curves show the shape of reverse S as a result of the influence by the shear deformation and slippage. In the loading cycle of the same displacement, the loads basically degenerate about 25 percent and the hysteretic loops display the semi-steady state. Hereafter, as the cyclic displacement increasing step by step, the unloading rigidity of the specimen degenerate more quickly, and the slippage was extremely serious owing to the spalling of the aerated concrete block, which were all reflected in the hysteretic curve as its middle part pinched seriously and approached closely to the displacement axis remaining the converse S shape.

(2) The difference between the hysteretic curves

The initial rigidity of the model wall EW1-2 is small while the others are large and about the same. Before the ultimate load, the rigidity of EW3-1 and EW3-2 decreased quickly while that of EW1-1 decreased most slowly. In the loading process of the same displacement before the ultimate load, the load of EW3-1 and EW3-2 degenerate quickly while EW1-1 degenerate more slowly. When arriving at 85% of the ultimate load, the hysteretic loops of the model walls (EW1-1, EW2-2 and EW3-2) show relatively full.

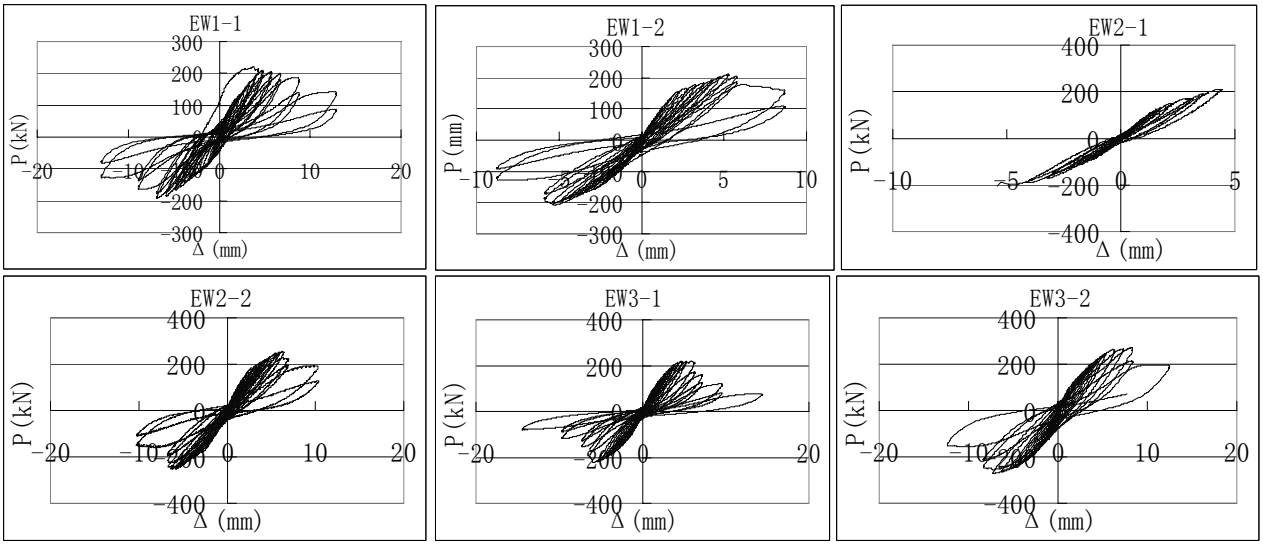

Figure 4 Hysteretic curves of model walls

(3) Conclusion ① For the specimen models, when multi-ribbed beams and columns were poured with fine stone concrete and the reinforcing steel bar increased, the energy dissipation wasn't improved as it was strengthened by pouring with the high strength mortar. ② For the specimen models, the more reinforcing steel

bars in the multi-ribbed beams and columns, the quicker the rigidity of the model walls degenerated as well as the load degenerated in the loading process of the same displacement.

3.2. Skeleton Curves of Shear Force and Displacement

The test characteristic values of the specimens under the low-cycle reversed horizontal loads are shown in Table 2. The quadrilinear restoring model was applied to represent the skeleton curves of the models as the nondimensional skeleton curves of the test under the same coordination seemed to be in good accordance with each other. The key points are respectively shown as: the cracking point A, the yield point B, the critical loading point C, the failure loading point D. the corresponding load and displacement as: the cracking load P_{cr}, the cracking displacement Δ_{cr}; the yield load P_y, the yield displacement Δ_y; the maximum load P_m; the corresponding displacement Δ_m; the ultimate load P_u; the ultimate displacement Δ_u.(Figure 5).

Table 2 The main seismic properties of multi-ribbed frame walls

Test wall	cracking		yield		critical		failure		Ductility factor
	P_{cr} (kN)	Δ_{cr} (mm)	P_y (kN)	Δ_y (mm)	P_m (kN)	Δ_m (mm)	P_u (kN)	Δ_u (mm)	
EW1-1	83	1.12	165.7	3.06	203.7	5.56	173.2	9.77	3.19
EW1-2	125	1.8	172.5	2.3	207.8	5.32	174.6	8.62	3.75
EW2-1	90.1	1.18	180	2.54	207.7	4.89	207.7	4.89	1.93
EW2-2	122.5	1.59	213.4	3.13	153.9	6.03	214.5	9.15	2.92
EW3-1	96.8	1.26	196.1	2.76	221.4	5.6	187.9	7.17	2.6
EW3-2	133.2	1.77	222.1	3.26	272	7.79	230.8	10.92	3.35

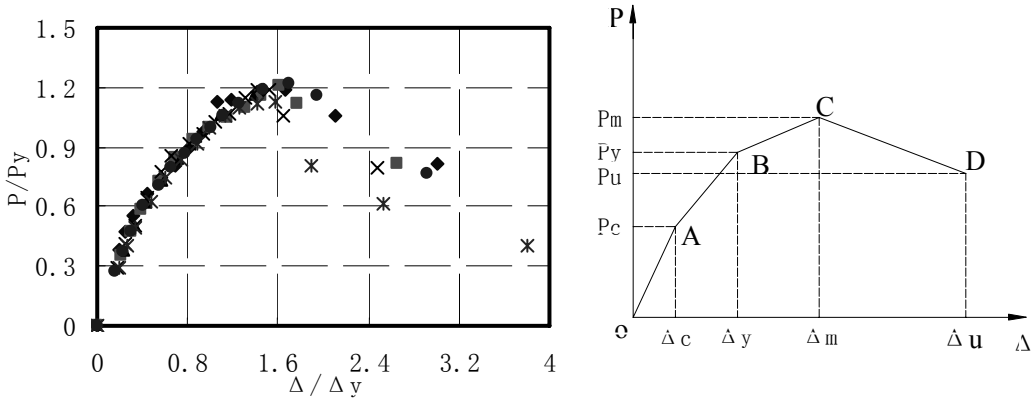

Figure 5 Skeleton curves of model walls

3.3. Definition of the Main Characteristic Points

The cracking point was defined as the corresponding point on the skeleton curve when the first group of obvious cracks formed. The value of the cracking point can be determined by the corresponding test data at the first turning point on skeleton curve. After the maximum load, the deformation increased rapidly while the load began to descend. Generally the ultimate load is defined as the load descends to about 85% maximum load and the corresponding deformation as the ultimate deformation. In fact the model walls haven't evident yield point, in order to discuss the deformation conveniently, the supposed yield point must be reasonably determined. The Park graphic analysis method was employed to analyze the skeleton curves of the model walls, and the supposed yield load was determined as $0.85\,P_m$, the corresponding lateral displacement as Δ_y.

3.4. Evaluation of the Ductility Capacity of Energy-saving Block and Invisible Multi-ribbed frame walls

Taking the lateral displacement Δ_y of the model walls at assumed yield point as its yield displacement, the average lateral displacement ductility factor of energy-saving block and invisible multi-ribbed frame walls calculated by test results is 3.16. The value illustrates the model walls rationally designed can meet seismic requirements of the structures. It can be seen from Table 2 that the ductility of the three model walls (EW1-1, EW1-2 and EW3-2) are fine, but the ductility descended instead of being strengthened along with the increasing of steel reinforcement. Therefore, although the failure mode of the model walls is mainly the shearing failure mode, the model walls rationally designed can still be with good deformability. The "rationally design" here refers to a rational shearing-compression ratio and arrangement the reinforcement of rib beams and columns.

4. RIGIDITY CALCULATIONS OF ALL STRESS STAGES AND RESTORING FORCE MODEL

4.1. Average Rigidity K_1 before Cracking

From the skeleton curves of energy-saving block and invisible multi-ribbed frame walls, it can be seen that before cracking integral performance of the model walls belong to the elastic condition basically. Therefore, the model wall with flanking wall may be simplified as I-shape section beam and obtained its average rigidity by elastic theory.

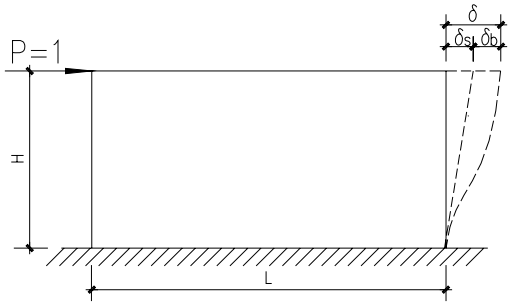

Figure 6 Flexural deformation and shearing deformation of model wall under a unit force

As shown in Figure 6 , the corresponding displacement signed by δ is called as lateral flexibility when a unit force is applied to the top end of the model wall, the lateral rigidity is the reciprocal of the lateral flexibility: $k = 1/\delta$.

Assuming there is no rotation occurred in the plane at the top and bottom end of the model wall, and under the unit horizontal force, the total deformation of the model wall

is composed of flexural deformation δ_b and shearing deformation δ_s. So the elastic lateral rigidity of the homogeneous model wall is:

$$K = \frac{1}{\delta_b + \delta_s} = \frac{1}{(\frac{H^3}{3EI} + \frac{\mu H}{GA})} \tag{4.1}$$

Where H represents the height of wall; the wall plane's area $A = Lt$, L is the wall length and t is the wall thickness; μ is the uneven coefficient of the model wall section shearing stress, for I-shape section $\mu = A / A'$, where A' is the web section area; $I = tL^3 / 12$ represents the section moment of inertia; E is the elastic modulus; G represents the shearing modulus.

The energy-saving block and invisible multi-ribbed frame wall structure is composed of energy-saving block and invisible multi-ribbed frame and the elastic modulus of two parts are different to a large extent, so the elastic lateral rigidity of the homogeneous model wall can't be directly calculated. The composite material method [3] was applied to deduce and calculate the elastic constants of the model wall. Thereby the elastic lateral rigidity can be calculated by the preceding formula (4.1); the results are shown in Table 3.

Table 3 Calculated results of the rigidity

Test wall	K_1(kN/mm)	K_0(kN/mm)	K_1/K_0
EW1-1	74.11	88.70	0.84
EW1-2	69.44	88.67	0.78
EW2-1	76.36	89.36	0.85
EW2-2	77.04	88.94	0.87
EW3-1	76.83	90.04	0.85
EW3-2	75.25	88.87	0.85

The rigidity before cracking of every piece of specimen was calculated by Equation (4.1). The calculated results are commonly higher than the test values and average high is about 15 percent. This is due to the slim cracks of energy-saving block and invisible multi-ribbed frame walls develop continuously before the visible cracks form. Therefore, Equation (4.1) must be modified as: $K_1 = 0.85K$

4.2. The Stiffness of the Model Walls after Cracking

After cracking the model walls start to show evident nonlinear performance, and the force transferring mechanism changes as well. At this time, the model walls confined by exterior frame form a resisting lateral force system consisted by the oblique-compression bar and the tension reinforcement. As the stress state is very complex, to solve theoretically the deformation of the model walls is of much difficulty. Therefore, the statistical method was applied to solve the stiffness of the model walls.

It can be seen from the skeleton curves in Figure 5, at four main characteristic points (the cracking point, the yield point, the critical point and the failure point), the lateral displacement and loading are respectively as follows: (1.44, 108.43), (2.84, 191.63), (5.87, 227.75) and (9.13, 196.2). Supposing the stiffness after cracking is $K_2 = \alpha_2 K_1$, the stiffness after yield is $K_3 = \alpha_3 K_1$ and the stiffness after the critical loading is $K_4 = \alpha_4 K_1$, it can be calculated from the geometric relation in Figure 5: $\alpha_2 = 0.68, \alpha_3 = 0.17, \alpha_4 = -0.13$.

4.3. The Restoring Model of Specimens

A gradual failure process was designed for the specimens, and the test process happened to demonstrate the design principle of energy–dissipation. Combining the skeleton curves and stiffness degeneration of the model walls, employing the rule[4-5] that the curve points to the maximum when the load is applied in opposite direction, the deteriorative quadrilinear restoring force model [6-7](see in Figure 7) is chosen in the paper as shown below.

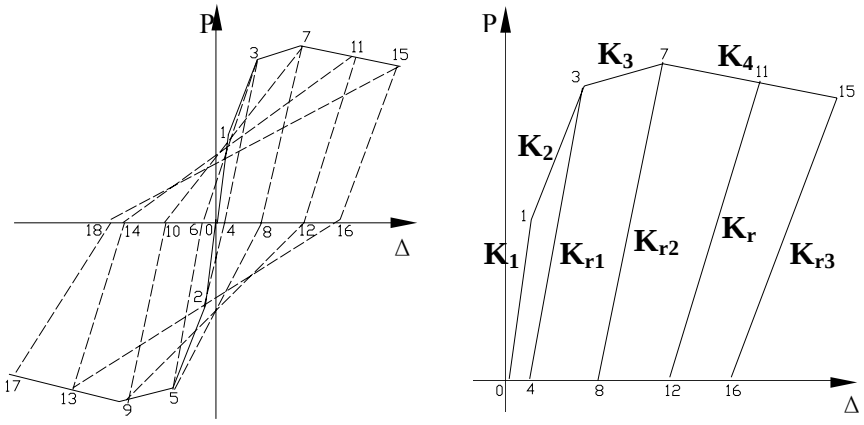

Figure 7 The restoring model of model walls

4.3.1. The loading stiffness

The transformation rule on the loading stiffness is shown in Figure7: the elastic stage (0-1) and the elastic stiffness K_1; the elastic-plastic stage (1-7), the stiffness K_2 before yield (1-3) and K_3 after yield (3-7); the failure stage (7-15) and the negative stiffness K_4. According to the data statistics of test results, the stiffness of every stage may adopt the prescription in section 4.2. The cracking point, yield point, maximum point, ultimate point are determined respectively according to the preceding definition and data statistics.

4.3.2. The unloading stiffness

The paper picked deteriorative quadrilinear model for the restoring model of model walls, the deteriorative rule of stiffness mainly relating to the unloading stiffness, as show in Figure 7. Based on the normal hysteretic loops obtained by statistics at the yield point, maximum point and ultimate point, the unloading stiffness of model walls at three stages may be constructed by interpolation. The formulas as follows (For an explanation of the symbols referring to 3.2):

$$K_r = (\Delta_{cr} / \Delta_r)^{0.5} K_1 \tag{4.2}$$

$$K_r = (\Delta_y / \Delta_r)^{0.61} K_1 \tag{4.3}$$

$$K_r = (\Delta_m / \Delta_r)^{0.63} K_1 \tag{4.4}$$

Where K_r represents the unloading stiffness and Δ_r is the lateral displacement of the model walls when unloaded.

5. CONCLUSIONS

(1) The average lateral displacement ductility factor of the energy-saving block and invisible multi-ribbed frame walls counted by test results is 3.16. This value illustrates that the model walls rationally designed can meet seismic requirements of the structure. Therefore, the general failure model of the model walls under low-cycle reversed lateral loads is shear failure model, but through rationally design, the model walls will still possess definite deformation capacity all the same.

(2) Through the fitting of the experimental data of energy-saving block and invisible multi-ribbed frame walls, the deteriorative quadrilinear restoring model of the model walls is obtained, which can reflect the hysteretic property and skeleton curves of the model walls comparatively correct. Therefore, the restoring model can be applied to the time-history analysis on the energy-saving block and invisible multi-ribbed frame structure.

(3) As the restoring model proposed in the paper is based on the pseudo static test, which can not comprehensively reflect the real dynamic performance of energy-saving block and invisible multi-ribbed frame walls. To comprehensively study the seismic performance exactly, the pseudo dynamic test or the shaking table test should be carried on.

REFERENCES

[1] Li, S.C., Zeng, Z.X. (2005). Research on energy-saving block and invisible multi-ribbed frame structure. In: Proceeding of the third specialty conference on the conceptual approach to structural design, Singapore: 119-124.

[2] Zhao, D., Yao, Q.F., Chen, P. (1999). Lateral rigidity calculation of multi-ribbed lightweight frame. *Journal of Xi'an University Architecture and Technology* **31:3**, 18-21. (in Chinese)

[3] Wang, Z.M. (2003). Composite Materials Mechanics and Composite Materials Structural Mechanics, Beijing, Science Press. (in Chinese)

[4] Zhang, X.P. (2003). The Nonlinear Analysis of Reinforced Concrete Seismic Structure, Beijing, Science Press. (in Chinese)

[5] Guo, Z.H., Shi, X.D. (2003). Principle and Analysis of Reinforced Concrete Seismic Structure, Beijing, Tsinghua University Press. (in Chinese)

[6] Huang, W., Yao, Q.F., Zhang, Y.M. (2005). Research of seismic performance and design theory of multi-ribbed slab wall. *Journal of Xi'an University Architecture and Technology* **37:1**, 34-39. (in Chinese)

[7] Yuan, Q., Yao, Q.F., Jia, Y.J. (2004). Numeric analysis on resisting blast capability of full closed steel-concrete-steel interlayer board. *Sichuan Building Science* **30:4**, 9-11, 23. (in Chinese)